Available online at www.sciencedirect.com
SCIENCE DIRECT
Combustion and Flame 142 (2005) 438–453
Combustion and Flame
www.elsevier.com/locate/combustflame

Turbulent lifted flames in a vitiated coflow investigated using joint PDF calculations

Renfeng Richard Cao [a,*], Stephen B. Pope [a], Assaad R. Masri [b]

[a] *Mechanical and Aerospace Engineering, Cornell University, 135 Upson Hall, Ithaca, NY 14853, USA*
[b] *School of Aerospace, Mechanical and Mechatronic Engineering, The University of Sydney, NSW 2006, Australia*

Received 13 September 2004; received in revised form 30 March 2005; accepted 9 April 2005

Available online 28 June 2005

Abstract

The joint velocity-turbulence frequency-composition PDF method is applied to a lifted turbulent jet flame with H_2/N_2 fuel issuing into a wide coflow of lean combustion products, which are at a temperature of 1045 K. Model calculations with detailed chemistry are performed using three existing mixing models (IEM, MC, and EMST) and two chemistry mechanisms (the Mueller and Li mechanisms). Numerically accurate results are obtained and compared with the experimental data. Recent experiments have shown that the stabilization height of this lifted flame is very sensitive to the coflow temperature, much more than to the inlet velocity profile or the initial temperature of the fuel. One percent (i.e., 10 K) change in the coflow temperature (which is well within the experimental uncertainty) can double the lift-off height. The joint PDF calculations capture this sensitivity very well and are in good agreement with the measurements for the velocity, mixture fraction, and species. The three mixing models give relatively similar results, implying that the cases studied here are mainly controlled by chemical kinetics. The Li mechanism results in earlier ignition than the Mueller mechanism and hence gives shorter lift-off heights over the whole test range. The joint PDF calculations generally give better agreement with the measurements than previous composition PDF calculations [A.R. Masri et al., Combust. Theory Modelling 8 (2004) 1–22]. A new parallel algorithm, involving domain partitioning of particles, has been implemented to facilitate these computations.

Keywords: PDF methods; Turbulent flames; Mixing models

1. Introduction

The probability density function (PDF) approach is now established as a numerical tool capable of modeling various important combustion phenomena relevant to practical combustion devices such as local extinction, reignition, and pollutant emissions [1–3]. The main advantage of this approach lies in the capability of handling nonlinear chemical reactions without approximation. Recent developments in the numerical method [4] have enabled detailed chemical kinetics to be used with reasonable computational costs. However, modeling mixing in PDF methods is still an open issue and the performance of the mixing models remains the subject of further investigations [5].

The three mixing models most widely used in PDF methods are the IEM model (Interaction by Exchange with the Mean) [6], which is identical to the

* Corresponding author. Fax: +1 607 255 1222.
E-mail address: rc239@cornell.edu (R.R. Cao).

0010-2180/$ – see front matter
doi:10.1016/j.combustflame.2005.04.005

Table 1
Experimental conditions studied by Cabra et al. [10] (the stoichiometric mixture fraction is $\xi_{st} = 0.47$, and X_{H_2} denotes the mole fraction of H_2, etc.)

	Diameter, D (mm)	Velocity, U (m/s)	Temperature, T (K)	X_{H_2}	X_{O_2}	X_{N_2}	X_{H_2O}
Jet	4.57	107	305	0.2537	0.0021	0.7427	0.0015
Coflow	210	3.5	1045	5×10^{-4}	0.1474	0.7534	0.0989

LMSE model [7], the MC model (Modified Curl) [8], and the EMST model (Euclidean Minimum Spanning Tree) [9]. For the simple test case of a partially stirred reactor, Ren and Pope [5] show that these three models can produce qualitatively and quantitatively different predictions. In this paper, the performance of these models is examined in joint PDF calculations of a lifted hydrogen jet flame in a vitiated coflow [10]. For each of these models, the rate of mixing is determined by the model constant C_ϕ, which represents the mechanical-to-scalar time-scale ratio. Previous studies show that PDF model calculations are sensitive to the value of C_ϕ [1,11]. In the present calculations, three different values of C_ϕ are employed in order to characterize the effects on the PDF calculations.

The flame studied here is a turbulent jet flame of H_2/N_2 issuing into a wide coflow of lean combustion products. This burner geometry, developed by Cabra et al. [10], provides a platform for studying complex lifted flames which may be undergoing autoignition. The burner simulates conditions, albeit with simple flows, that are encountered in gas turbine combustors and furnaces where there is a recirculation of hot combustion products. Extensive data [10,12–15] now exist for selected flames stabilized on the Cabra burner enabling it to become a model problem for validating calculations. The experimental condition studied by Cabra et al. [10] and detailed in Table 1, is taken as the base case in the current work.

Earlier calculations of the flame with the same conditions listed in Table 1, have been reported by Masri et al. [16] and Cabra et al. [10] using the composition PDF approach. The calculations of Masri et al. [16] use the CFD package, FLUENT, with the MC mixing model and show that this flame is largely controlled by autoignition.

The characteristics of these flames were recently investigated by Wu et al. [12] and Gordon et al. [17] for different operating conditions, e.g., coflow temperature, coflow velocity, and jet velocity. It is found that the stabilization height is very sensitive to the coflow temperature. This sensitivity is a challenging modeling problem for numerical calculations.

This paper represents the first velocity-composition joint PDF calculations of this flame, and the first study of the comparative performance of all three mixing models in application to a turbulent flame. The Li mechanism [18] for hydrogen chemistry is used, and its performance is compared with that of the Mueller mechanism [19]. Calculations are performed over a range of operating conditions, which include not only those investigated experimentally [12,17] but also other conditions such as different jet temperatures and inlet turbulence levels. Some comparisons between the present joint PDF calculations and the previous composition PDF calculations [16] are also shown.

In the next section, the submodels used in the joint PDF calculations are briefly introduced and the values of the model constants are given. Then the numerical method is outlined, and the steps taken to ensure the numerical accuracy of the calculations are described. The results of the calculations are then presented and compared to the experimental data. Conclusions are drawn in the final section.

2. The joint velocity-turbulence frequency-composition PDF method

The particle implementation of the joint PDF method requires models for mixing, velocity and turbulent frequency following a fluid particle [20]. Various Langevin models have been developed [21–23] for the evolution of the particle velocity to account for the acceleration due to the mean pressure gradient and to provide a closure for the effects of viscous dissipation and the fluctuating pressure gradient. The SLM (Simplified Langevin Model) [21], which is the simplest, is used in the present calculations. The model constant C_0 is set to $C_0 = 2.1$.

The turbulent frequency is a particle property which provides the time scale of turbulence. Here we use the stochastic frequency model of Van Slooten et al. [23] with the constants set to their standard values: $C_{\omega 1} = 0.65$, $C_{\omega 2} = 0.9$, $C_3 = 1.0$, $C_4 = 0.25$, and $C_\Omega = 0.6893$. The turbulence models used are the same as those used in many previous studies, e.g., [24,25].

In PDF methods, the effect of molecular diffusion on the composition is represented by a mixing model. Three different mixing models, IEM, MC, and EMST, are implemented in the calculations. The mix-

ing model constant C_ϕ is traditionally set to 2.0, but different values have also been used in previous PDF calculations. Using the EMST model, Xu and Pope [1] observe the correct level of local extinction in joint PDF calculations of the Barlow and Frank [26] flames (D, E, and F) when the value $C_\phi = 1.5$ is used. On the other hand, using the MC model, Lindstedt et al. [11] suggest the value $C_\phi = 2.3$ in their calculations of the same flames. This value is also used by Lindstedt and Louloudi [3] in the calculations of four pilot-stabilized turbulent jet flames investigated experimentally by Masri and co-workers [27]. In the present work, the influence of C_ϕ is examined by performing calculations with the values $C_\phi = 1.5$, 2.0, and 2.5 for each of the mixing models.

In addition to the micro-mixing process, a particle's composition also changes due to chemical reaction. An accurate mechanism is necessary to describe combustion chemistry particularly for a flame involving strong turbulence-chemistry interactions. Two chemistry mechanisms are used in the current calculations. The first one is the hydrogen mechanism developed by Mueller et al. [19] which involves 10 species (H_2, H, O, O_2, OH, H_2O, HO_2, H_2O_2, Ar, N_2) and 21 reactions. The second mechanism by Li et al. [18] involves the same species as the Mueller mechanism with modifications to some of the thermodynamic and kinetic data.

3. Numerical solutions

There are several implementations of particle-mesh methods to solve the modeled joint PDF equations. All computations presented here use a code named HYB2D [25] which implements a hybrid FV/particle algorithm. In the hybrid algorithm, the PDF/particle method (particle part) is coupled with a finite volume solver (FV part). The FV part solves the mean conservation equations for mass, momentum, energy, and the mean equation of state; and the particle part solves the fluctuating velocity-turbulent frequency-composition PDF transport equations. The FV calculations provide mean fields of velocity, density, and pressure to the particle part and obtain the turbulent fluxes and mean reaction source term from the particle calculations. The algorithm is fully consistent at the level of differential equations, but not at the numerical level (because of truncation error and other numerical errors). Correction algorithms developed by Muradoglu et al. [25] are used to guarantee consistency of the duplicate fields at all levels.

The flow considered here is statistically 2D axisymmetric and nonswirling. A polar-cylindrical (z, r) coordinate system is used with the origin at the center of the fuel jet at its exit plane. The computational domain is rectangular, of extent $(0, 15D)$ in the radial direction, and $(0, 50D)$ in axial direction, where D is the diameter of the jet ($D = 4.57$ mm).

The inlet velocity profile is taken either from measurements [15] or from earlier calculations of Masri et al. [16]. The velocity covariance is specified via the correlation coefficient ρ_{uv}: between $r = 0$ and $r = R \equiv 0.5D$, ρ_{uv} varies linearly from 0 to 0.4; for $1 \leqslant r/R \leqslant 2.87$, ρ_{uv} equals 0.4; and for $r/R > 2.87$, ρ_{uv} is zero. The remaining covariances are assumed to be zero for this nonswirling axisymmetric flow. The ratio of production to dissipation is specified as unity which, together with the specified profiles, determines the inlet profile of mean turbulence frequency. Consequently Ω is set to zero for $r/R > 2.87$. This has negligible impact on the calculations, since the values of Ω within the jet are up to five orders of magnitude larger than those at $r/R = 2$; and Ω is calculated as a conditional mean in which values of Ω below the mean $\langle\Omega\rangle$ are excluded [28]. The temperature, composition, and density are specified as being uniform in each stream in accord with the experimentally determined values (see Table 1). A trace amount of Argon is added to the fuel and this is used to determine mixture fraction. This is done for convenience: the mixture fraction can also be determined from other conserved scalars. The coflow boundary ($r = 15D$) is treated as a perfect-slip wall. Symmetry conditions are applied on the centerline ($r = 0$). At the exit plane, in the FV part, the mean density and the axial and radial mean velocities are extrapolated from the interior, and the pressure is specified.

A parallel algorithm, named "domain partitioning of particles," has been developed and implemented by Cao et al. [29]. To explain this algorithm, let us consider a PDF simulation performed in parallel using N processors. The FV grid partitions the solution domain into n_{cell} cells. These cells are distributed into N subdomains, each consisting of approximately n_{cell}/N cells and each assigned to a different processor. There are a total of N_{p} particles, with each cell containing approximately $N_{\text{pc}} = N_{\text{p}}/n_{\text{cell}}$ particles. At the beginning of each time step, all of the particles in a cell are stored on the same processor, namely the processor which is assigned to the subdomain containing the cell. During the time step (on convection substeps) particles can move from cell to cell and some may move to cells in different subdomains. At the end of the time step, message passing (using MPI) is performed to transfer particles that have moved from their initial subdomain to the processor corresponding to their current subdomain.

In this domain partitioning of particles, since all of the particles in a given cell are stored on the same processor, it is simple to implement particle interaction models (e.g., Curl's model or EMST) on the

full ensemble of particles in a cell. So, this algorithm has the advantages of reducing the bias related both with particle-mean-field interactions and with particle-particle interactions. It has been verified that the parallel and serial computations yield statistically identical results. Note, however, that only the particle part of the code is parallelized: the same FV computation is performed on each processor. The method is effective in reducing the turnaround time by a factor of 15 when 30 processors are used. Load balancing and communication overhead issues need to be resolved to achieve higher parallel efficiency and further reductions in turnaround time.

Numerical accuracy is crucial in modeling studies of turbulent reactive flows. The discrepancy between the calculated results and the reliable experimental results has two ingredients: the modeling error, caused by deficiencies in the physical and chemical models, and the numerical error caused by the solution algorithms. To investigate the performance of the physical and chemical models, the numerical error must be below acceptable levels. The following paragraphs describe the efforts to minimize the numerical errors which are controlled by the following parameters: (i) the ISAT (In-Situ-Adaptive Tabulation) [4] error tolerance, (ii) the number of cells in the domain, (iii) the number of particles per cell, (iv) the coefficients of the numerical viscosity, and (v) the coefficients of time averaging.

ISAT is used for the implementation of the detailed chemistry. The error incurred in retrieving from the ISAT table is controlled by the specified error tolerance ϵ_{tol}. When retrieving is not possible and the ODEs are integrated numerically, the associated numerical error is controlled by the specified ODE error tolerance. The effects of the ISAT and ODE error tolerances have been studied systematically by Masri et al. [16]. Since essentially the same ISAT and chemical mechanism are used in the present work, the same parameters, i.e., ISAT and ODE error tolerances of 6.25×10^{-6} and 1×10^{-8}, respectively, are used here. This guarantees that the tabulation error results in less than 2% error in the conditional mean temperature at the stoichiometric mixture fraction [16], a quantity which is found to be very sensitive to such errors.

Grid convergence is examined using grid sizes from 24×24, 48×48, 68×68, 96×96 to 136×136. The 96×96 grid is used for all the present calculations. This results in errors no greater than 1% (with respect to the peak value) for the mean temperature and major species, and 5% for the minor species.

The effect of the average number of particles per cell N_{pc} is studied with $N_{\text{pc}}=25$, 50, and 100 for all the three mixing models separately on the coarsest grid 24×24. The discrepancy between the results for $N_{\text{pc}}=50$ and $N_{\text{pc}}=100$ is around 1% for temperature and the major species and about 6% for the minor species. The value $N_{\text{pc}}=100$ is used in all subsequent calculations.

The FV solver involves two numerical viscosity coefficients ν_2 and ν_4. Numerical viscosities are added as dissipative terms in the numerical scheme of the current finite-volume solver [30]. The dissipative terms are constructed as an adaptive blend of second and fourth order differences and are needed to stabilize the scheme so that it converges to a steady-state solution. Calculations on the 96×96 grid with three different sets of numerical viscosities were performed and the results show that the discrepancy between them is less than 0.5% for the mean temperature and major species, and about 3% for the minor species. In the calculations reported here, the values used are $\nu_2=0.25$ and $\nu_4=2.0$, the same as those used in previous calculations [28,31].

In the current HYB2D code, a loosely coupled hybrid algorithm using pseudo-time stepping is implemented [25] and time averaging is used to reduce the statistical error in the final results. It takes about 500 steps for particles initially in the domain to be swept out of the domain. Typically, more than 6000 time steps (in the particle part) are used for time averaging, and this corresponds to about 12 flowthrough times. The time-averaging factor used in the moving time average increases from 20 to 1200 from the beginning to the end of this process. The purpose of performing extensive time averaging is to minimize the effect of statistical fluctuations which (with time averaging) are less than 0.5% for mean temperature and major species and 2% for the means of minor species. Another reason is that a calculation of 6000 particle time steps can be performed in one day due to the implementation of parallel processing algorithms.

4. Results and discussion

The computations presented in this section use the 96×96 grid with 100 particles per cell. Mean quantities are obtained by averaging over more than 6000 time steps. The ISAT and ODE error tolerances are set to 6.25×10^{-6} and 1.0×10^{-8}, respectively. These conditions were found by Masri [16] to yield numerically accurate calculations.

4.1. The experiments

The composition and velocity measurements referred to in this paper were performed, respectively, at Sandia National Laboratories and the University of Sydney. Stability measurements by Wu et al. [12] and Gordon et al. [17], presented in Fig. 1, show that the lift-off height of these flames, H/D, is very sensitive

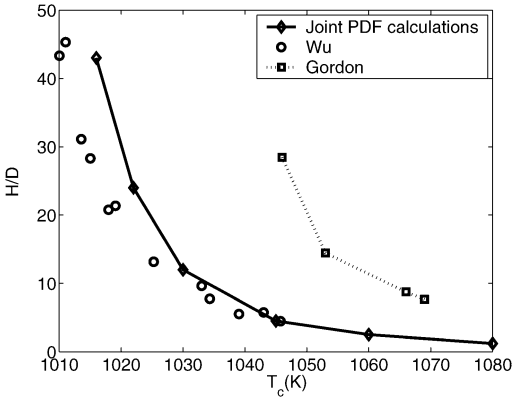

Fig. 1. Measured and computed lift-off height using different values of coflow temperature. (Circles) Measurements of Wu et al. [12]; (dotted line with squares) measurements of Gordon et al. [17]; (line with diamond) joint PDF calculations using the EMST mixing model and the Li mechanism.

to the temperature of the coflow (T_c) such that a decrease of 10 degrees in T_c can double the value of H/D. These two sets of temperature measurements were made at different times with different thermocouples, and the differences between the two sets of results are within the expected error from thermocouple measurements which, at these temperatures, is of the order of 30 K [10]. Using advanced laser diagnostics to measure temperatures (T_c) in the coflow would be extremely useful and this is planned for future experiments.

Given this high sensitivity to T_c, the flame lift-off height is used instead as a qualitative marker of similar flames that have the same fuel jet velocity. As an example, composition measurements were made at Sandia for a flame with $T_c = 1045$ K which corresponds to a lift-off height of $H/D \approx 10$. Based on the measurements of Wu et al. [12], to obtain a flame with the same lift-off height at the University of Sydney, the coflow temperature had to be reduced to about $T_c = 1022$ K [15]. Flow-field measurements were then made in this flame which is now taken as the Sydney University representation for Sandia's $T_c = 1045$ K case.

Measurements in nonreacting flows [13] have shown that the surrounding air begins to affect the jet at about $z/D = 25$, where the uniform coflow temperature profile is diminished. Because of the differences between the nonreacting case and reacting cases, the location of the point where the surrounding air begins to affect the jet may be different for the reacting case, but it may still be somewhere around $z/D = 25$. In the current calculations, a wide coflow is used to provide a uniform coflow environment without a surrounding air stream. Hence comparisons between calculations and experimental data are only relevant in regions of the flow upstream of the location where the cold air begins to affect the jet (i.e., for $z/D \leqslant 25$).

4.2. Effect of the boundary conditions

4.2.1. Effect of the coflow temperature

Fig. 1 also shows a sample calculation for the lift-off heights computed for a range of coflow temperatures using the EMST mixing model and the Li mechanism. It is clear that while the trends are similar to the experimental measurements, the absolute lift-off heights are different and this may be due to a combination of experimental errors, numerical errors, and different definitions of the lift-off height. This implies that in order to make sensible comparisons between calculations and measurements (as well as between calculations), flames are selected to have the same lift-off height but not necessarily the same coflow temperature. For example, for further comparison with the measurements in the Sandia flame ($T_c = 1045$ K and $H/D \sim 10$), Fig. 1 shows that a lift-off height of $H/D = 10$ in these calculations corresponds to a coflow temperature of 1033 K.

Experimentally [12,17], the stabilization height was obtained from digital images of flame emission recorded at the flame base. This emission arises mainly from water as well as other species such as OH. To facilitate comparison with experimental data, a relevant numerical criterion needs to be defined for lift-off height. For the same flame studied here, Cabra et al. [10] reported that at the visible lift-off region, the measured mass fraction of OH reaches about 2×10^{-4}. This criterion is adopted here and the lift-off height, H, is defined numerically as the first axial location, z, at which the Favre mean mass fraction of OH reaches a value of 2×10^{-4} (at any radius). Further comparison of measured and calculated lift-off heights are reported below (Figs. 8 and 10).

Experimental data [10] as well as the current calculations indicate that the ignition zone is generally located off the axis at a radial position $r \approx 5$ mm. Axial profiles at this radial location are, therefore, used to investigate the effects of the coflow temperature on the lift-off height. Fig. 2 shows a comparison of the measured with computed axial profiles (off the axis at $r = 5$ mm) of Favre mean and rms temperature, and mass fraction of OH and H_2O. Coflow temperatures of $T_c = 1022$, 1030, 1038, 1045, 1060, and 1080 K are used for these computations. It is clear that as the coflow temperature increases, the flame ignites sooner and the ignition point moves toward the jet exit plane. The lift-off heights obtained using $T_c = 1060$ K and $T_c = 1080$ K are very close to each other. A further increase in the coflow temperature has a small effect on the flame. Fig. 2 confirms that the flame is very sensitive to the temperature in the coflow making

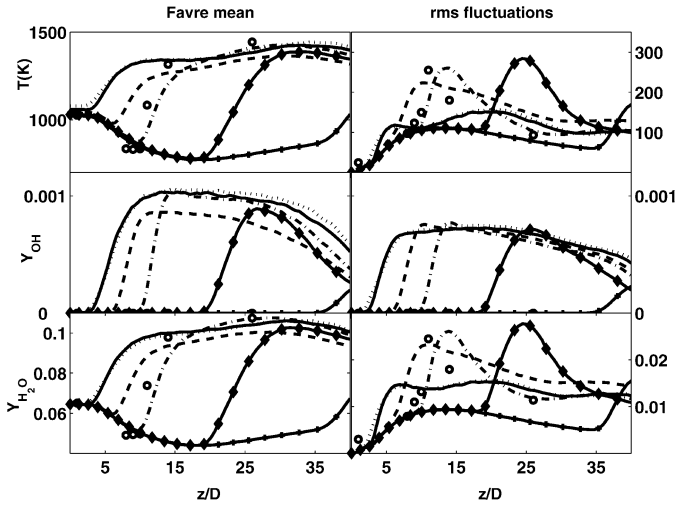

Fig. 2. Axial profiles (off the axis at $r = 5$ mm) of Favre mean (left plots) and rms (right plots) temperature, and mass fractions of OH and H_2O. (Circles) Measurements [13]; (lines) PDF calculations using the Mueller mechanism and the EMST mixing model with different values of the coflow temperature T_c. (Solid line with plus) $T_c = 1022$ K; (solid line with diamond) $T_c = 1030$ K; (dash dot) $T_c = 1038$ K; (dash) $T_c = 1045$ K; (solid) $T_c = 1060$ K; (dot) $T_c = 1080$ K.

it extremely hard to obtain absolute agreement with measurements given that the experimental uncertainty in the temperature data is 3% [10].

4.2.2. Effect of the inlet velocity profiles

Two different inlet velocity profiles are used in this paper and shown in Fig. 3. One inlet velocity profile is taken from previous calculations by Masri et al. [16] for the Sandia flame with $T_c = 1045$ K. These calculations used the composition PDF approach and

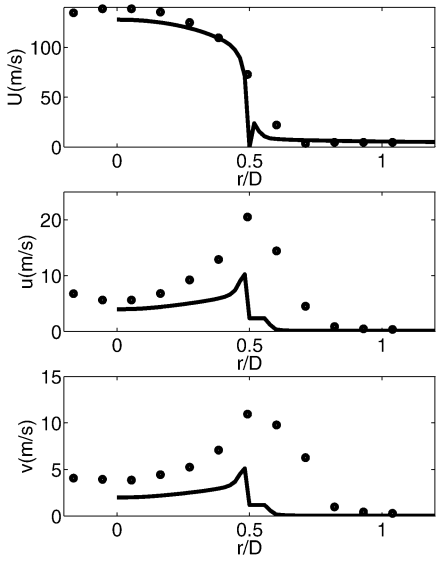

Fig. 3. Measured and calculated inlet velocity profiles. (Symbols) The measured velocity profiles [15]; (lines) the calculated velocity profiles [16].

were initiated further upstream of the exit plane. The computed velocity profiles at $x/D = 0$ are used here and these are referred to as the "computed inlet velocity profiles." The second set of inlet velocity profiles is measured at the University of Sydney for the flame with $T_c = 1022$ K [15]. These are referred to as the"measured inlet velocity profiles." Two observations can be made from Fig. 3. First, the computed centerline mean axial velocity is lower than the measured centerline velocity by about 7%. Second, the computed peak rms fluctuation of velocities are about half of the measured values. The possible reason is that the turbulence intensity of 10% used in the boundary condition of the composition PDF calculations may be lower than the actual value.

Calculations are performed here for a flame with the same fuel jet velocity of 107 m/s and $T_c = 1033$ K but with different inlet velocity profiles; namely the "computed" and"measured" inlet velocity profiles. Both calculations use the EMST mixing model and the Li mechanism. Results are shown in Fig. 4 in the form of radial profiles for the mean axial velocity and its rms fluctuations. The calculations using the measured inlet velocity profiles yield better agreement with the experimental data for the mean velocity, but the calculations that use the computed inlet velocity profiles show better agreement with the measured rms fluctuations of velocity.

Also shown on Fig. 4 are previous calculations performed by Masri et al. [16] using the composition PDF approach and corresponding joint PDF calculations using the MC mixing model and the Mueller mechanism. It is notable here that the current joint

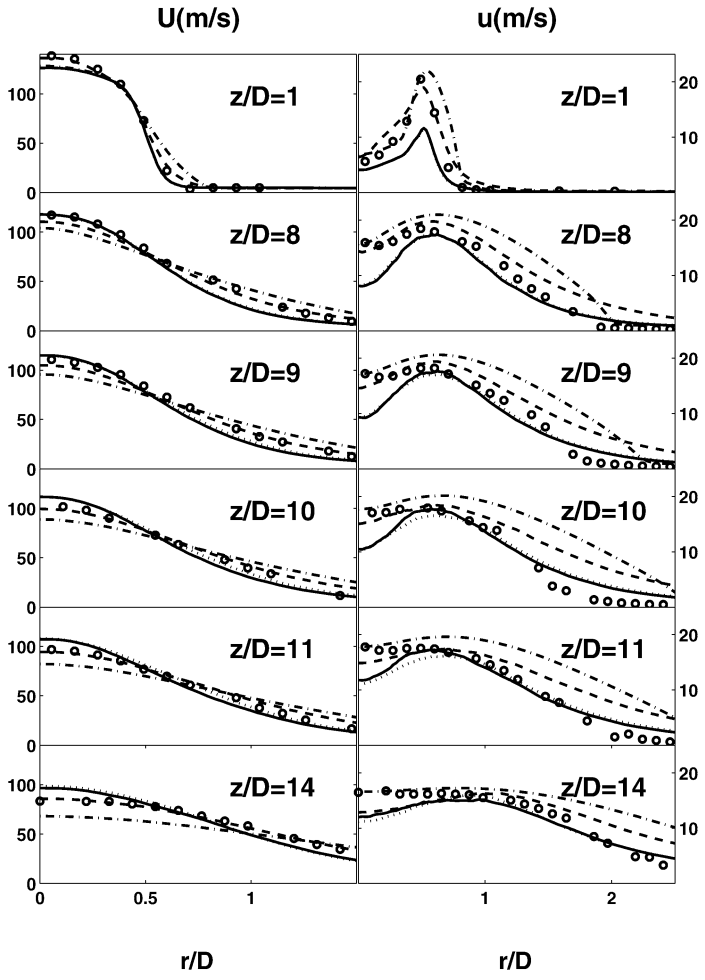

Fig. 4. Radial profiles of mean (left plots) and rms (right plots) axial velocity. (Circles) Measurements [15]; (solid line), joint PDF calculations with the computed inlet velocity profiles (EMST, Li, $T_c = 1033$ K); (dash line) joint PDF calculations with the measured inlet velocity profiles (EMST, Li, $T_c = 1033$ K); (dash-dotted line) composition PDF calculations [16] (MC, Mueller, $T_c = 1045$ K); (dotted line) joint PDF calculations with all conditions the same as those of the composition PDF calculations (MC, Mueller, $T_c = 1045$ K).

PDF calculations result in improved mean velocities and rms fluctuations, even at $z/D = 1$, compared to the composition PDF approach. Further investigation about the effect of the inlet velocity profiles is shown in Section 4.6.

4.2.3. Effect of the inlet turbulence intensity

The effect of the inlet turbulence intensity is investigated by changing the amplitude of the inlet (both the jet and coflow) velocity fluctuations. The contour plots of the Favre mean mass fraction of OH are shown in Fig. 5. The LHS plot is obtained using the standard calculated inlet velocity rms while the RHS plot is obtained using twice this value. The location of the base of the flame is almost the same for both cases. However, significant differences in the subsequent development of the flame may be observed. Further comparisons are shown in Fig. 6 including one additional calculation using half of the standard calculated inlet velocity fluctuations. Axial profiles for Favre means of mixture fraction, temperature, and the mass fraction of OH are plotted for two radial locations of $r = 0$ and $r = 5$ mm. It is clear that the initial turbulence level affects the mixing at downstream locations in the jet and hence the temperature and composition fields.

Different inlet velocity fluctuations, and hence different turbulence intensities, change the effect of macro-mixing between the jet and the coflow and consequently change the profiles of mixture fraction and temperature. In the range $z/D < 10$, the change of OH is mainly controlled by the reaction instead of by

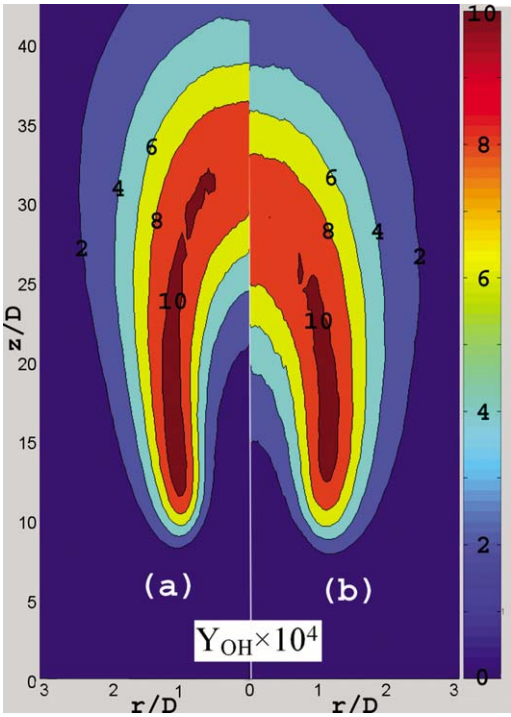

Fig. 5. Contour plots of the Favre mean mass fraction of OH obtained using joint PDF calculations (MC, Mueller mechanism, $T_c = 1045$ K) with different inlet velocity fluctuations. (a) Standard calculated inlet velocity fluctuation profiles; (b) inlet velocity fluctuation doubled.

macro-mixing, so the OH profiles are almost the same and the locations of the flame bases are approximately the same for the three cases with different inlet velocity fluctuations. Large differences can be observed in the OH profiles further downstream because significant amounts of OH have been produced and both the reaction and the macro-mixing affect the local concentration of OH.

Table 2
Lift-off heights obtained using different boundary conditions

Effect of jet temperature			
Jet temperature (K)	290	305	320
Lift-off height (H/D)	9.8	8.5	7.0
Effect of jet velocity			
Jet velocity (m/s)	96	107	170
Lift-off height (H/D)	8.1	8.5	11.2
Effect of coflow velocity			
Coflow velocity (m/s)	3.5	7.0	10.5
Lift-off height (H/D)	8.5	10	14

4.2.4. Effect of other inlet boundary conditions

Unlike the coflow temperature, other boundary conditions, i.e., the coflow velocity, jet temperature, and jet velocity, have little effect on this flame. A summary of the numerical test results is shown in Table 2.

For the jet temperature, a 5% change results in less than 20% change in the lift-off heights. This effect is much smaller than that of the coflow temperature, which can double the lift-off height with only 1% change. The lift-off height increases slowly with the

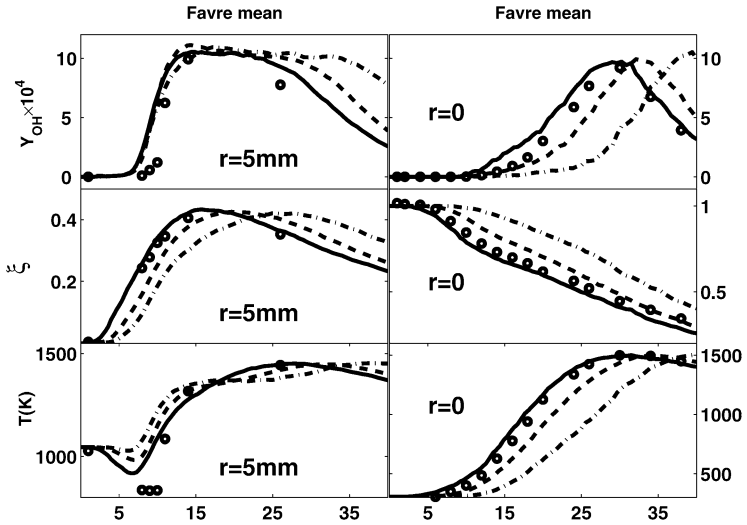

Fig. 6. Axial profiles off the axis at $r = 5$ mm (left plots) and centerline profiles (right plots) of the Favre mean mass fraction of OH, mixture fraction and temperature. (Circles) Measurements [13]; (lines) joint PDF calculations (MC, Mueller mechanism, $T_c = 1045$ K) with different inlet velocity fluctuations. (Dashed line) Standard calculated inlet velocity fluctuations; (dash-dotted) half of the standard calculated inlet velocity fluctuations; (solid) double the standard calculated inlet velocity fluctuations.

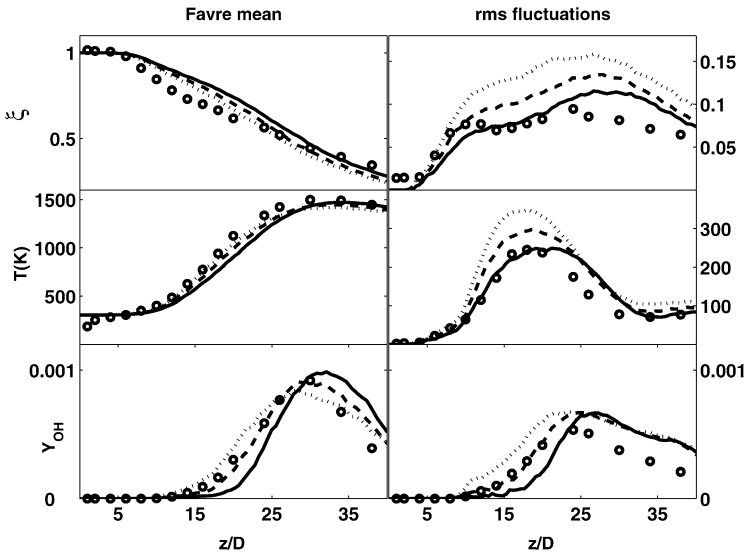

Fig. 7. Axial profiles on the centerline ($r = 0$) of Favre mean (left plots) and rms (right plots) mixture fraction, temperature, and mass fraction of OH. (Circles) Measurements [13]; (lines) PDF calculations with $T_c = 1045$ K, using the Mueller mechanism and the EMST mixing model with $C_\phi = 1.5$ (dotted), 2.0 (dashed), and 2.5 (solid).

increase of the jet velocity and coflow velocity in the calculations.

For the jet velocity, this tendency is qualitatively the same as the measurements [12,17]. However, for the coflow velocity, the calculations and measurements give different trends. In the calculations, the lift-off height increases monotonically with the coflow velocity. On the other hand, the measured lift-off heights [12] reach a maximum value for a coflow velocity of 4.5 m/s. Further increases in coflow velocity result in a decrease in the lift-off height. More investigation is needed to understand this discrepancy.

4.3. Effect of C_ϕ and the comparison of mixing models

4.3.1. Effect of C_ϕ

Masri et al. [16] have shown in their composition PDF calculations that this flame is largely chemically controlled and the value of the mixing model constant C_ϕ has a relatively small effect. It is expected that this is also true for the joint PDF calculations. Fig. 7 shows the axial profiles for the Favre mean and rms mixture fraction, temperature, and mass fraction of OH computed for the lifted flame using different values of C_ϕ. As expected, an increase in C_ϕ results in a decrease in the rms fluctuations of mixture fraction.

More investigations of the effect of C_ϕ are performed by calculating the lift-off height over a series of coflow temperatures and the results are shown in Fig. 8. Once again we find that the effect of C_ϕ is relatively small compared to the effect of the coflow temperature. The lift-off heights obtained using different values of C_ϕ are almost identical for coflow temperatures higher than 1030 K. The difference becomes obvious when the coflow temperature decreases to 1022 K. An increase in the value of C_ϕ results in stronger mixing in composition space which facilitates reaction and hence reduces the lift-off height. (The lift-off heights obtained using $T_c = 1022$ K are much larger than $H/D = 25$. At these downstream locations, the flame penetrates the hot coflow cone and is subsequently affected by the surrounding air.)

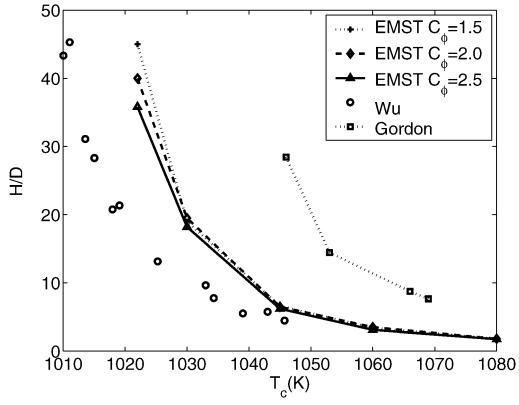

Fig. 8. Lift-off height against coflow temperature. (Circles) Measurements of Wu et al. [12]; (dotted line with square) measurements of Gordon et al. [17]; (lines) joint PDF calculations using the EMST mixing model and the Mueller mechanism with the mixing model constant $C_\phi = 1.5$ (dotted line with cross), 2.0 (dashed line with diamond), and 2.5 (solid line with triangle).

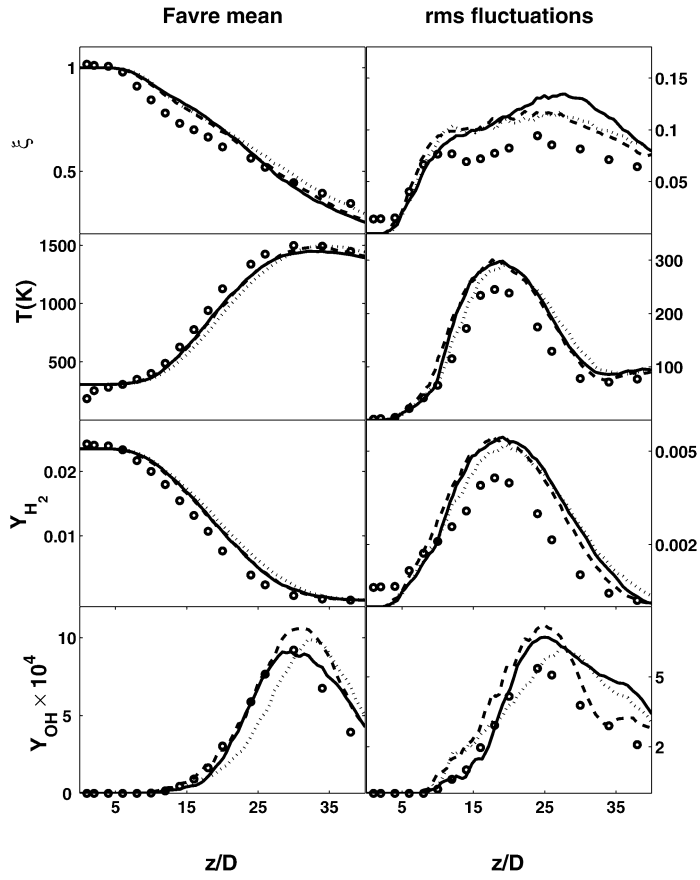

Fig. 9. Axial profiles on the centerline ($r = 0$) of Favre mean (left plots) and rms (right plots) mixture fraction, temperature, and mass fraction of H_2 and OH. (Circles) Measurements [13]; (lines) PDF calculations with $T_c = 1045$ K, using the Mueller mechanism and different mixing models. MC (dotted), IEM (dashed), EMST (solid).

The EMST mixing model is used in the above calculations. The effect of C_ϕ is also tested (but not shown) for the MC and IEM mixing models with the coflow temperature set to 1045 K: the tendency is similar to that of the EMST mixing model. Since the effect of C_ϕ is relatively small for all mixing models, the standard value ($C_\phi = 2.0$) is used for all subsequent calculations presented in this paper.

4.3.2. Comparison of mixing models

Fig. 9 compares measured centerline profiles of the Favre mean and rms of mixture fraction, temperature, and the mass fraction of H_2 and OH computed using the MC, IEM, and EMST mixing models. It can be seen that all calculations are in reasonable agreement with the experimental data. The differences between different mixing models are small except for the profiles of OH. For the Favre mean OH, the calculation using the MC mixing model is significantly different than those of the IEM and EMST mixing models. The peak value obtained using IEM is about 20% higher than that of EMST calculations. Significant differences can also be observed for the rms fluctuations of OH. However, all of these differences are quite small and much less than the difference corresponding to 1% change in the coflow temperature. At some locations these differences are of the same order as the experimental and computational uncertainties, so it is not evident (from these results) that one mixing model is distinctly superior to the others.

Further investigations of the performance of the mixing models are made by performing a series of calculations using different values of coflow temperature and the results are shown in Fig. 10. The EMST calculations give shorter lift-off heights than the IEM calculations over the whole range of tested coflow temperatures. The MC calculations give the largest lift-off heights at most coflow temperatures but a crossover occurs with the IEM and EMST calculations at coflow temperatures of about 1028 and 1022 K for the Mueller and Li mechanisms, respectively.

For the calculations obtained using the same mechanism, the differences in the lift-off heights be-

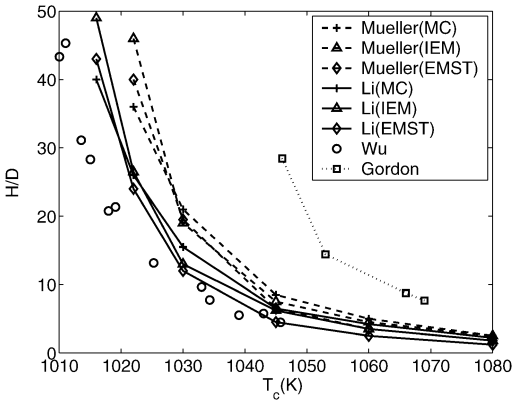

Fig. 10. Lift-off height against coflow temperature. (Circles) Measurements of Wu et al. [12]; (dotted line with square) measurements of Gordon et al. [17]; (lines) joint PDF calculations using Mueller mechanism (solid line) and Li mechanism (dashed line) with different mixing models. MC (line with cross); IEM (line with diamond); EMST (line with triangle).

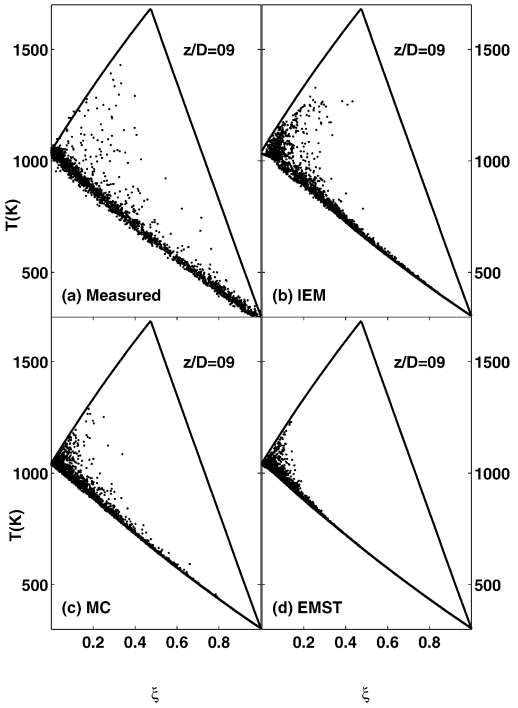

Fig. 11. Measured and computed scatter plots of temperature against mixture fraction for lifted flame at $z/D = 9$. (a) Experimental data [13]. (b–d) Computed using IEM ($T_c = 1033$ K), MC ($T_c = 1040$ K), and EMST ($T_c = 1038$ K) mixing models, respectively. The Mueller mechanism is used for these calculations. The upper solid line is the equilibrium temperature.

tween different mixing models are generally less than $3D$, where D is the jet diameter. But it can reach up to $10D$ in the low coflow temperature range. It is also worth noting that the differences in the calculated lift-off heights due to different mixing models are smaller that the differences due to different chemistry mechanisms.

Figs. 11–14 show scatter plots for temperature versus mixture fraction at four different axial location in the flames. In each figure, a measured scatter plot is shown along with three others calculated using the IEM, MC, and EMST mixing models. The Mueller mechanism is used for these calculations. The solid lines shown on each plot represents the equilibrium temperature. To compare the performance of different mixing models, the coflow temperature is adjusted in the calculations so that ignition occurs at the same location as that of the measurements [10]. The coflow temperatures needed to achieve this are $T_c = 1033$, 1040, and 1038 K for IEM, MC, and EMST mixing models, respectively.

The reasons that this flame is insensitive to different mixing models can be explained by Fig. 11 showing results at $z/D = 9$ which is just upstream of the ignition point. At this location, both measurements and calculations show almost all fluid samples lying on the inert mixing line between $(\xi, T) = (0, 1045\ \text{K})$ and $(\xi, T) = (1, 305\ \text{K})$. And, it may be seen that these samples are continuously distributed in the ξ–T space. Of course, different mixing models yield somewhat different distributions along the mixing line but all models yield a significant amount of ignitable mixture. The subsequent autoignition is controlled by the chemistry and this is the dominant rate-controlling process.

The insensitivity of this flame to different mixing models is relative to its high sensitivity to the coflow temperature. Significant difference can still be observed for calculations using different mixing models in the mean axial profiles (Fig. 9), the scatter plots at $z/D = 11$, 14, and 26 (Figs. 12–14), and the calculation of lift-off heights (Fig. 10). But all of these differences are small when compared to the differences caused by 1% change in the coflow temperature (Figs. 1 and 10).

Further downstream, at $z/D = 11$, Fig. 12 shows that a significant proportion of fluid samples is igniting or already ignited and this is occurring mostly on the lean side of stoichiometric. At $z/D = 14$, as may be seen from Fig. 13, in the experiments the lean mixtures ($\xi < 0.3$, say)are mainly fully burnt. The same is true for the calculations with IEM and EMST, but with MC there are unburnt and partially burnt samples.

Different characteristics of the mixing models may be seen from Figs. 12–14. The IEM results show bimodal behavior with a lean band ($\xi < 0.5$ in Fig. 12

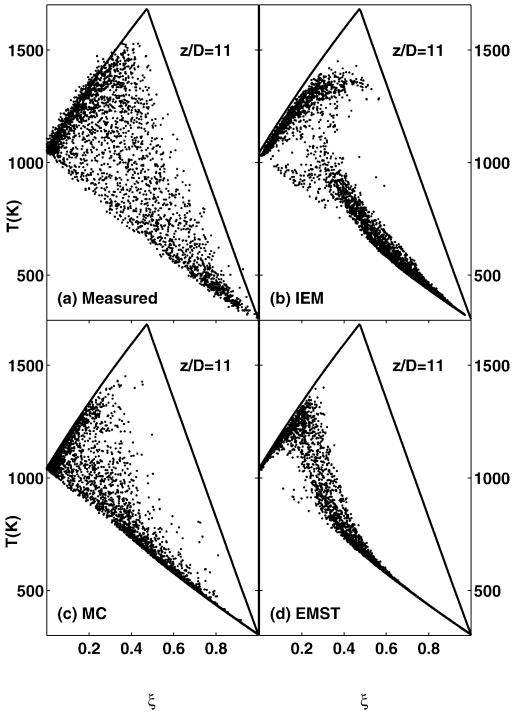

Fig. 12. Measured and computed scatter plots of temperature against mixture fraction for lifted flame at $z/D = 11$. (a) Experimental data [13]. (b–d) Computed using IEM ($T_c = 1033$ K), MC ($T_c = 1040$ K), and EMST ($T_c = 1038$ K) mixing models, respectively. The Mueller mechanism is used for these calculations. The upper solid line is the equilibrium temperature.

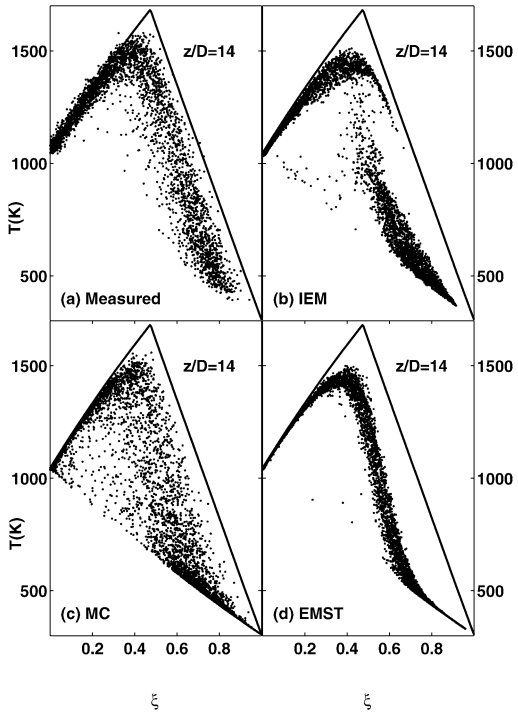

Fig. 13. Measured and computed scatter plots of temperature against mixture fraction for lifted flame at $z/D = 14$. (a) Experimental data [13]. (b–d) Computed using IEM ($T_c = 1033$ K), MC ($T_c = 1040$ K), and EMST ($T_c = 1038$ K) mixing models, respectively. The Mueller mechanism is used for these calculations. The upper solid line is the equilibrium temperature.

and $\xi < 0.6$ in Fig. 13) of reacted fluid, and a rich band ($\xi > 0.2$ in Fig. 13 and $\xi > 0.4$ in Fig. 12) of largely unreacted fluid. The MC results show a wide distribution between the unreacted and the reacted states and generally have better agreement with the measurements, especially on the fuel-rich side. However, in Fig. 13, it may be seen that the calculations based on the EMST mixing model are in accord with the experimental data for $\xi < 0.7$ (although the width of the scatter band is somewhat narrower). In particular, for $\xi < 0.6$, there are almost no points on or close to the inert mixing line. In contrast, both the IEM and the MC results show a significant amount of mixed but unreacted fluid (e.g., for $\xi = 0.4$). The EMST results have narrower bands in the T–ξ space and have less reacted points on the fuel-rich side than the measurements.

Another observation from Figs. 11–14 is that this flame is far from equilibrium for stoichiometric and rich mixtures even at the downstream location with $z/D = 26$. To a large extent the calculations show the same lack of equilibrium as the measurements, especially at stoichiometric. Since equal diffusivities are assumed in the calculations, differential diffusion may not be responsible for the suppression of the flame temperature on the rich side. This effect is, presumably, either because of the interaction of mixing and reaction, or simply because reaction is slow to achieve equilibrium.

4.4. Comparison of chemistry mechanisms

The Li mechanism is an updated version of the Mueller mechanism which includes some improved thermodynamic data and rate constants. Fig. 10 clearly shows that the Li mechanism calculations ignite sooner than the Mueller mechanism calculations and hence give shorter lift-off heights over the whole test range. With increasing coflow temperature, the differences in the lift-off heights between the calculations using the two different mechanisms diminish.

It is clear from Figs. 8 and 10 that the choice of mixing models or the specification of the mixing model constant C_ϕ ($C_\phi = 1.5$, 2.0, or 2.5) has less effect on the calculated lift-off heights than the chemical kinetic mechanisms. This is consistent with previous findings [16].

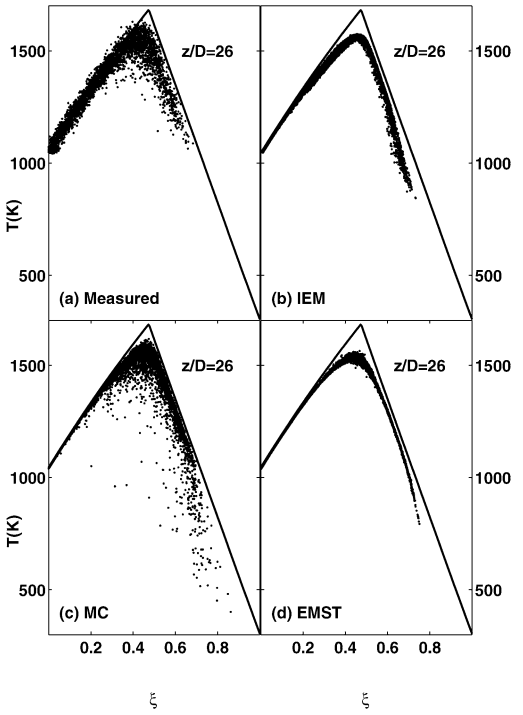

Fig. 14. Measured and computed scatter plots of temperature against mixture fraction for lifted flame at $z/D = 26$. (a) Experimental data [13]. (b–d) Computed using IEM ($T_c = 1033$ K), MC ($T_c = 1040$ K), and EMST ($T_c = 1038$ K) mixing models, respectively. The Mueller mechanism is used for these calculations. The upper solid line is the equilibrium temperature.

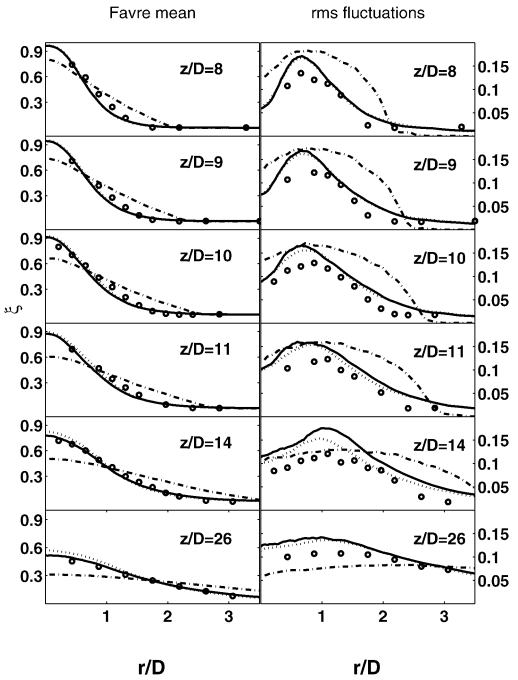

Fig. 15. Radial profiles of Favre mean (left plots) and rms (right plots) mixture fraction. (Circles) Measurements [13]; (dash-dotted line) composition PDF calculations (MC, Mueller mechanism, $T_c = 1045$ K); (dotted line) joint PDF calculations with the same settings as those of composition PDF calculations (MC, Mueller mechanism, $T_c = 1045$ K); (solid line) joint PDF calculations using the EMST mixing model, the Mueller mechanism, and coflow temperature $T_c = 1033$ K. The computed inlet velocity profiles are used for all calculations in this figure.

4.5. Comparison of joint PDF and composition PDF calculations

The superior performance of the joint PDF approach has already been demonstrated in Fig. 4 where the calculated radial profiles of mean axial velocity and rms fluctuations are clearly closer to measurements that those obtained from the composition PDF. These two approaches are further contrasted here with respect to the mixing field. Fig. 15 shows measured and calculated radial profiles of the Favre mean mixture fraction and its rms fluctuations. Calculations using the joint velocity-composition PDF are considerably more accurate than the previous composition PDF calculation which overpredicts the spreading and mixing rates. It is worth noting here that the composition PDF approach uses the k–ϵ turbulence model with the standard coefficients and this is well known to yield excessive spreading of round jets.

The capability of the joint PDF calculations to yield better agreement compared with the measurements for both the velocity and the mixture fraction fields is a significant advantage over the composition PDF approach. This is particularly relevant for downstream locations in the jets where this latter approach fails even if the k–ϵ constants are modified. It should be noted here that the use of more advanced versions of the k–ϵ model or a Reynolds-stress turbulence model may yield improved calculations using the composition PDF. However, the joint PDF approach is more likely to compute the correct flow and mixing fields in more complex flows which involve swirl and recirculation. This improved calculation of the flow and mixing field results in good agreement with the measurements for the composition field as is demonstrated in the next section.

4.6. Calculation of scalar fields

This section validates the performance of the joint PDF approach with respect to reactive scalar fields. The measured and calculated temperature and species mass fractions are compared at various axial locations in the flames. As discussed earlier, and given the strong sensitivity of this flame to the coflow temperature and experimental uncertainty associated with

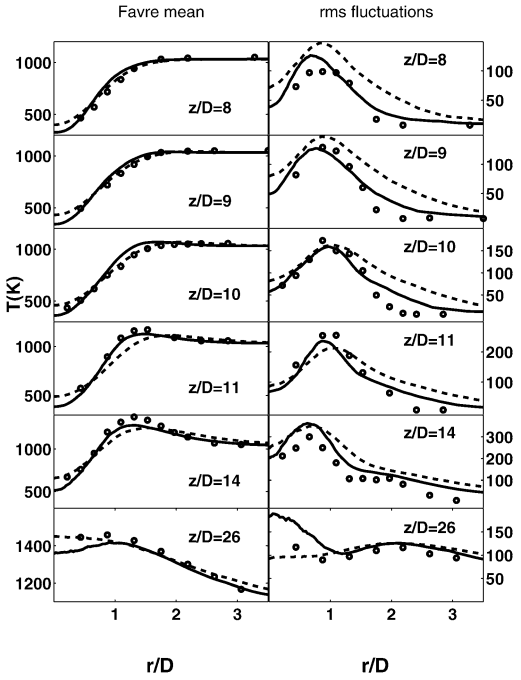

Fig. 16. Radial profiles of Favre mean (left plots) and rms (right plots) temperature. (Circles) Measurements [13]; (lines) joint PDF calculations (EMST, Li mechanism) obtained using calculated inlet velocity profiles [16] (solid line, $T_c = 1033$ K) and measured velocity profiles [15] (dashed line, $T_c = 1031$ K).

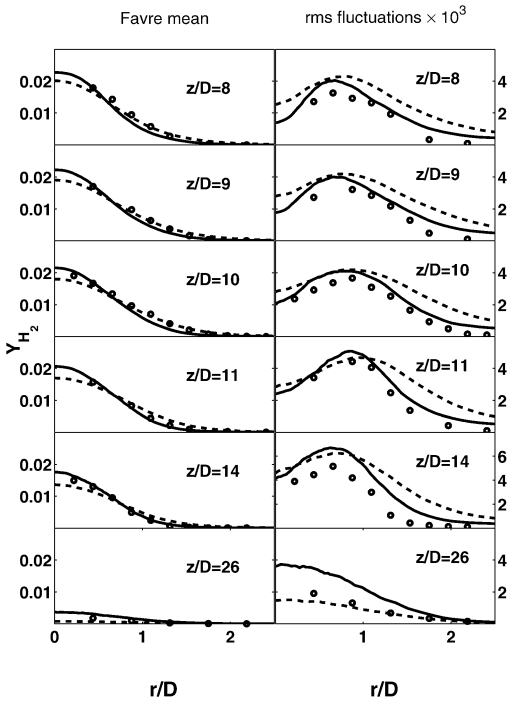

Fig. 17. Radial profiles of Favre mean (left plots) and rms (right plots) mass fraction of H_2. (Circles) Measurements [13]; (lines) joint PDF calculations (EMST, Li mechanism) obtained using calculated inlet velocity profiles [16] (solid line, $T_c = 1033$ K) and measured velocity profiles [15] (dashed line, $T_c = 1031$ K).

its measurement, it is more appropriate to make comparisons between flames that have the same lift-off height rather than at the same coflow temperature. Measurements are available for a flame with a coflow temperature of $T_c = 1045$ K and a lift-off height of about 10 diameters. To match this lift-off height using the PDF approach, a coflow temperature of $T_c = 1031$ K is needed if the calculated inlet velocity profiles are used. A slightly higher coflow temperature of $T_c = 1033$ K is required when the measured inlet velocity profiles is employed. It is worth noting here that the difference of 12–14 K in T_c is still small compared to the experimental uncertainty of 31 K (3%). It can also be noted that in an independent experiment under the same nominal conditions, Kent [15] found that $T_c = 1022$ K yielded the same lift-off height as that observed by Cabra et al. [10].

Figs. 15–20 show the radial profiles of Favre mean and rms mixture fraction, temperature, and mass fraction of H_2, O_2, H_2O, and OH. The Li mechanism and the EMST mixing model are used for these calculations; $T_c = 1033$ K is used for the computed inlet velocity profiles [16] and $T_c = 1031$ K is used for the measured inlet velocity profiles [15]. One can see that the joint PDF calculations using the computed inlet velocity profiles are generally in better agreement with the measurements, for both the mean and the rms profiles. At the same time, calculations using measured velocity profiles yield comparable results in the mean profiles, but overpredict the rms profiles in most plots. This may be caused by two reasons. First, from Fig. 4 one can see from the velocity profiles that the calculations using the measured inlet profiles overpredict the rms velocity at $z/D > 8$. This overprediction in the rms velocity results in an overprediction in the rms species profiles. Second, it should be noted here that while inlet velocity profiles have some impact on the calculated flame structure, this remains relatively small compared to the effects of the coflow temperature.

5. Conclusions

In the present work, numerically accurate velocity-turbulent frequency-composition joint PDF calculations have been made for the first time for a turbulent lifted flame issuing in a vitiated coflow. The effects of the boundary conditions are investigated. Model calculations with detailed chemistry are performed using three existing mixing models, i.e., IEM, MC, and EMST. Two detailed hydrogen mechanisms, i.e.,

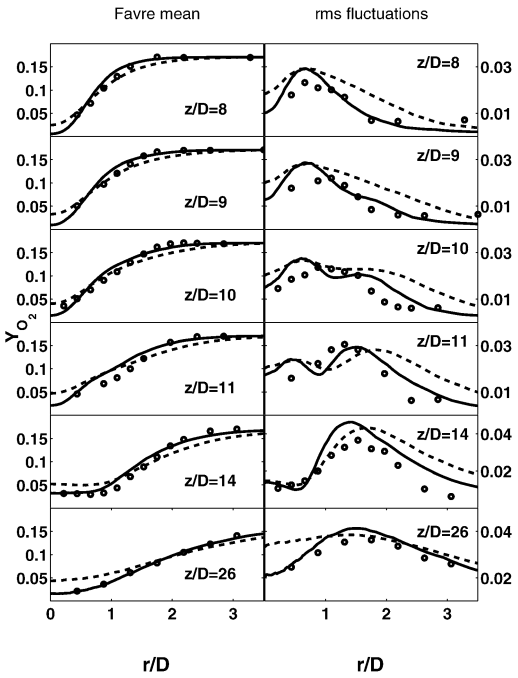

Fig. 18. Radial profiles of Favre mean (left plots) and rms (right plots) mass fraction of O_2. (Circles) Measurements [13]; (lines) joint PDF calculations (EMST, Li mechanism) obtained using calculated inlet velocity profiles [16] (solid line, $T_c = 1033$ K) and measured velocity profile [15] (dashed line, $T_c = 1031$ K).

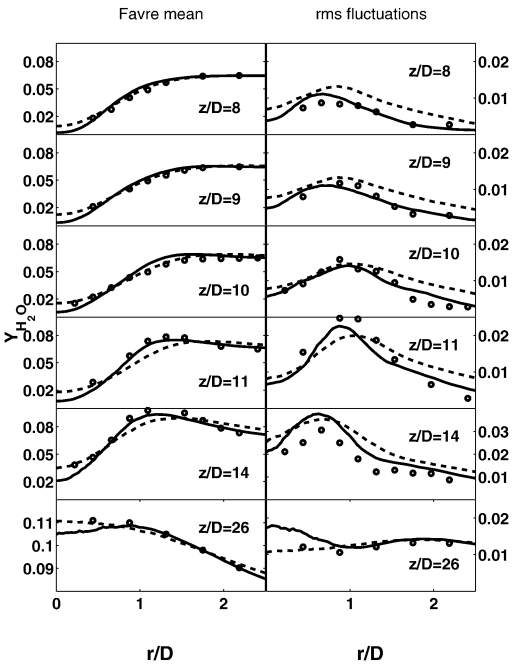

Fig. 19. Radial profiles of Favre mean (left plots) and rms (right plots) mass fraction of H_2O. (Circles) Measurements [13]; (lines) joint PDF calculations (EMST, Li mechanism) obtained using calculated inlet velocity profiles [16] (solid line, $T_c = 1033$ K) and measured velocity profiles [15] (dashed line, $T_c = 1031$ K).

the Mueller and Li mechanisms, are implemented using ISAT. This is the first study of the comparative performance of all three mixing models in application to a turbulent flame with detailed chemistry. A new parallel algorithm, involving domain partitioning of particles, has been implemented. The calculated velocity, temperature and reactive scalar fields are compared with measurements.

Two inlet velocity profiles are used in the calculations to compare with the scalar field measurements. Good agreement with measurements is shown for the velocity, mixture fraction, temperature, and species. The calculations using computed inlet velocity profiles yield better agreement with the measured scalar profiles, especially for the rms profiles.

Generally, the velocity field and mixture fraction profiles are not very sensitive to the boundary conditions (including the coflow temperature), mixing models, and chemistry mechanisms. On the other hand, temperature and the reactive scalar fields are very sensitive to the coflow temperature and this is captured very well by the joint PDF calculations presented here. Given this strong sensitivity to the coflow temperature, T_c, comparisons are made between flames which have the same lift-off height rather than the same T_c.

There are various indicators pointing to the conclusion that this flame is largely chemistry controlled: (i) the use of different mixing models and different values of the mixing model constant C_ϕ ($C_\phi = 1.5$, 2.0, and 2.5) has much less effect on this flame than varying the chemical kinetic mechanism or the coflow temperature; (ii) the turbulence intensity specified at the inlet boundary affects profiles of velocity, temperature, and mixture fraction but does not significantly affect the species controlling the chemistry at upstream locations in the flame, so that the lift-off height remains largely unaffected; (iii) it can be seen from the scatter plots (e.g., Fig. 11) that there are many mixed, potentially reactive but unreacted points located on the inert mixing line.

Calculations using the EMST mixing model give shorter lift-off heights than those with the IEM model. Calculations using the MC mixing model give the highest lift-offs for most coflow temperatures, but a crossover between the IEM and EMST calculations occurs at a coflow temperature about 1028 and 1022 K for the Mueller and Li mechanisms, respectively. The Li mechanism yields earlier ignition than the Mueller mechanism and hence gives shorter lift-off heights over the whole test range. The current joint PDF calculations exhibit better agreement with the

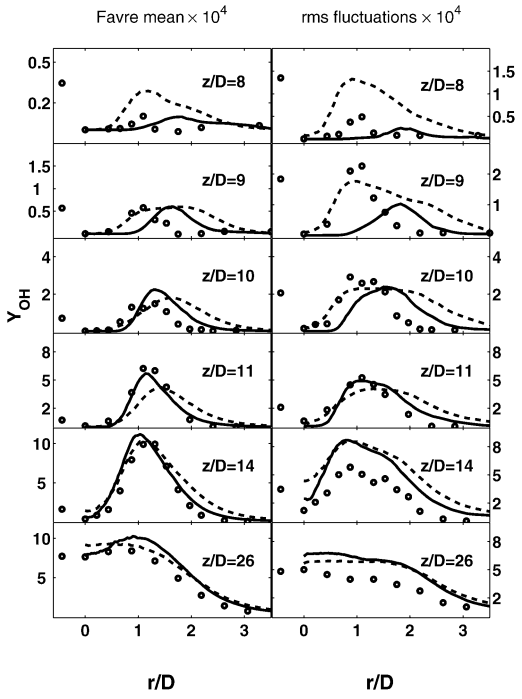

Fig. 20. Radial profiles of Favre mean (left plots) and rms (right plots) mass fraction of OH. (Circles) Measurements [13]; (lines) joint PDF calculations (EMST, Li mechanism) obtained using calculated inlet velocity profiles [16] (solid line, $T_c = 1033$ K) and measured velocity profiles [15] (dashed line, $T_c = 1031$ K).

experimental data than the previous composition PDF calculations. The composition PDF method overpredicts the spreading of the velocity and mixture fraction because of the use of the k–ϵ turbulence model with standard coefficients.

Acknowledgments

This work is supported by Air Force Office of Scientific Research under Grant F-49620-00-1-0171. Professor Masri is supported by the Australian Research Council. The computations were conducted using the resources of the Cornell Theory Center, which receives funding from Cornell University, New York State, federal agencies, foundations, and corporate partners.

References

[1] J. Xu, S.B. Pope, Combust. Flame 123 (2000) 281–307.
[2] Q. Tang, J. Xu, S.B. Pope, Proc. Combust. Inst. 28 (2000) 133–139.
[3] R.P. Lindstedt, S.A. Louloudi, Proc. Combust. Inst. 29 (2002) 2147–2154.
[4] S.B. Pope, Combust. Theory Modelling 1 (1997) 41–63.
[5] Z. Ren, S.B. Pope, Combust. Flame 136 (2004) 208–216.
[6] J. Villermaux, J.C. Devillon, in: Proc. Second Int. Symp. on Chemical Reaction Engineering, Elsevier, New York, 1972.
[7] C. Dopazo, E.E. O'Brien, Acta Astronaut. 1 (1974) 1239–1266.
[8] J. Janicka, W. Kolbe, W. Kollman, J. Non-Equilibrium Thermodyn. 4 (1977) 47–66.
[9] S. Subramaniam, S.B. Pope, Combust. Flame 115 (1998) 487–514.
[10] R. Cabra, T. Myhrvold, J.Y. Chen, R.W. Dibble, A.N. Karpetis, R.S. Barlow, Proc. Combust. Inst. 29 (2002) 1881–1888.
[11] R.P. Lindstedt, S.A. Louloudi, E.M. Vaos, Proc. Combust. Inst. 28 (2000) 149–156.
[12] Z. Wu, S.H. Starner, R.W. Bilger, in: D.R. Honnery (Ed.), Proceedings of the 2003 Australian Symposium on Combustion and the Eighth Australian Flame Days, The Combustion Institute, 2003.
[13] R. Cabra, R.W. Dibble, http://www.me.berkeley.edu/cal/VCB/ (2002).
[14] A.R. Masri, R.W. Bilger, http://www.aeromech.usyd.edu.au/thermofluids/ (2003).
[15] J.E. Kent, B.E. thesis, The University of Sydney (2003).
[16] A.R. Masri, R. Cao, S.B. Pope, G.M. Goldin, Combust. Theory Modelling 8 (2004) 1–22.
[17] R.L. Gordon, S.H. Starner, A.R. Masri, R.W. Bilger, to be presented at the Fifth Asia–Pacific Conference on Combustion, Adelaide University, Australia, 2005.
[18] J. Li, Z. Zhao, A. Kazakov, F.L. Dryer, in: Fall Technical Meeting of the Eastern States Section of the Combustion Institute, Penn State University, University Park, PA, October 26–29, 2003.
[19] M.A. Mueller, T.J. Kim, R.A. Yetter, F.L. Dryer, Int. J. Chem. Kinet. 31 (1999) 113–125.
[20] S.B. Pope, Prog. Energy Combust. Sci. 11 (1985) 119–192.
[21] D.C. Haworth, S.B. Pope, Phys. Fluids 29 (1986) 387–405.
[22] S.B. Pope, Phys. Fluids 6 (1994) 973–985.
[23] P.R. Van Slooten, Jayesh, S.B. Pope, Phys. Fluids 10 (1998) 246–265.
[24] P. Jenny, M. Muradoglu, K. Liu, S.B. Pope, D.A. Caughey, J. Comput. Phys. 169 (2001) 1–23.
[25] M. Muradoglu, S.B. Pope, D.A. Caughey, J. Comput. Phys. 172 (2001) 841–878.
[26] R.S. Barlow, J.H. Frank, Proc. Combust. Inst. 27 (1998) 1087–1095.
[27] A.R. Masri, R.W. Dibble, R.S. Barlow, Combust. Flame 89 (1992) 167–185.
[28] M. Muradoglu, K. Liu, S.B. Pope, Combust. Flame 132 (2003) 115–137.
[29] R. Cao, D.A. Caughey, S.B. Pope, in: Fall Technical Meeting of the Eastern States Section of the Combustion Institute, Penn State University, University Park, PA, October 26–29, 2003.
[30] D.A. Caughey, AIAA J. 7 (1988) 26–841.
[31] K. Liu, S.B. Pope, D.A. Caughey, Combust. Flame 141 (2005) 89–117.